Journal of The Electrochemical Society, **147** (2) 687-698 (2000)
S0013-4651(99)05-082-X CCC: $7.00 © The Electrochemical Society, Inc.

Computational Aspects of Laser Radiometric Multiparameter Fit for Carrier Transport Property Measurements in Si Wafers

M. E. Rodriguez,[a,c,z] A. Mandelis,[a] G. Pan,[a] L. Nicolaides,[a] J. A. Garcia,[a] and Y. Riopel[b,*]

[a]*Photothermal and Optoelectronic Diagnostics Laboratories, Department of Mechanical and Industrial Engineering, University of Toronto; and Materials and Manufacturing Ontario, Toronto, Ontario, M5S 3G8, Canada*
[b]*MITEL SCC, Bromont, Quebec JOE 1LO,Canada*

A laser infrared photothermal radiometric (PTR) multiparameter-fit methodology has been developed to obtain unique measurements of the thermal and electronic parameters of industrial-type Si wafers. The influence of recombination lifetime, front, and back surface recombination velocities, carrier electronic diffusion coefficient, thermal diffusivity (α), as well as of the total plasma and thermal contributions to the PTR signal as a function of frequency is examined computationally and experimentally in this paper. Silicon wafers with low and high resistivity were studied with the proposed methodology. A strong correlation between nominal resistivity, front surface recombination velocity, and recombination lifetime was found: higher resistivity wafers are likely to have lower surface recombination velocity and longer lifetimes. The first PTR lifetime scanned image of subsurface electronic defects has also been produced.
© 2000 The Electrochemical Society. S0013-4651(99)05-082-X. All rights reserved.

Manuscript submitted May 20, 1999; revised manuscript received September 9, 1999.

A computational multiparameter fitting methodology that uses a three-dimensional laser photothermal radiometric model for semiconductors is presented in this study. One- and three-dimensional models of the free-carrier plasma-wave generation and response to laser photothermal (PT) excitation in a semiconductor have been reported in the literature.[1,2] The amplitude of PT response in these models has been used to measure carrier transport properties of electronic materials. The total radiation emitted from a silicon sample illuminated with a modulated laser beam arises from two sources: emission of IR radiation from the photoexcited carrier plasma-wave (injected excess carrier density) and from direct lattice photon absorption and optical-to-thermal (nonradiative) power conversion leading to temperature rise (a thermal wave).[1,3] Sheard and co-workers[1,2] observed experimentally that under infrared photothermal radiometric (PTR) detection, carrier emission dominates and the thermal-wave contribution can be neglected for some Si samples. This observation was addressed theoretically by Salnick *et al.*[4,5] These authors generated a composite plasma- and thermal-wave PTR model of semiconductors and showed that the plasma-wave signal component can dominate in high-quality materials virtually at all modulation frequencies. However, in this model the radial spatial variation of laser-generated excess carriers and of the temperature rise was not considered. Ikari *et al.*[6] have recently presented a general theoretical model for the laser-induced PTR signal from a semiconductor wafer of finite thickness using a three-dimensional geometry. In this model, carrier diffusion and recombination, as well as heat conduction, along the radial and axial directions in the sample were taken into account using cylindrical coordinates. A pair of conventional coupled plasma- and heat diffusion-wave equations were written and solved in Hankel space. In this theoretical framework, the plasma and thermal components can be written as follows

$$S_{\mathrm{PTR}}(\omega) = \frac{C_1}{A}\int_0^\infty F(\lambda,\omega)J_1(\lambda a)d\lambda + \frac{C_2}{A}\int_0^\infty T(\lambda,\omega)J_1(\lambda a)d\lambda \quad [1]$$

In Eq. 1, A is the effective detector area: $A = \pi a^2$, where a is the detector radius; $J_1(x)$ is the Bessel function of the First Kind and order one; and $F(\lambda, \omega)$ and $T(\lambda, \omega)$ are the radial Hankel transforms of corresponding frequency-dependent solutions to the plasma-wave and thermal-wave boundary-value problems under optical excitation by a Gaussian laser beam. These functions have been reported previously.[5,6] They contain the thermal and electronic transport parameters of the electronic solid: recombination lifetime (τ), minority carrier diffusion coefficient (D_n), front surface recombination velocity (S_1), back surface recombination velocity (S_2), and thermal diffusivity (α). In practice, for accurate measurements, both thermal-wave and plasma-wave contributions must be considered in the interpretation of PTR data (amplitude and phase) from semiconductor samples, such as Si wafers. The electronic quality of industrial semiconductor wafers varies widely, and they frequently exhibit strong thermal behavior, especially at low modulation frequencies. The PTR technique is an excellent candidate for nondestructive multiparameter measurements in electronic materials because it can offer measurements of the foregoing important properties, which are crucial for device fabrication control. The major problem, facing the implementation of the three-dimensional model by Ikari *et al.*[6] for use with experimental radiometric data, is the reliability of the measured values of any and all of the aforementioned electronic transport parameters, in view of the intrinsic nonuniqueness of the theoretical fit (maximum of five unknown material parameters plus the constants C_1 and C_2 in Eq. 1) to only two data channels (amplitude and phase) available to the experimenter.

In this paper we present a computational methodology developed to address precisely the unique problem of the PTR signal interpretation. The effects of the various transport parameters on the shape of the frequency response curves (amplitude and phase) are studied theoretically first. Then a robust computational best-fit algorithm is described, based on the specifics of signal sensitivity dependence on a given transport parameter across particular regions of the modulation frequency spectrum. As a result, the conditions for unique fits and reliable parameter measurements are deduced and examples of such measurements are given, including the first cerrier-lifetime scanned images of deep subsurface damage in a wafer.

Theoretical Simulations

A pair of conventional coupled plasma and heat diffusion equations based on Eq. 1 can be written and solved in Hankel space. The computational methodology is described in the Appendix. The three-dimensional (3D) PTR signal is finally obtained by taking a weighted superposition of the plasma and thermal contributions[3]

$$S_{\mathrm{PTR}}(\omega) = C_p S_{\mathrm{Plasma}}(\omega) + C_t S_{\mathrm{Thermal}}(\omega) \quad [2]$$

where parameters C_p and C_t represent the weight of each component (plasma and thermal) contributing to the PTR signal, and S_{PTR} represents a vector in the sense of a function with a complex argument. In Eq. 2, the plasma-wave component (S_{plasma}) is obtained from the

* Electrochemical Society Active Member.
[c] On leave from: Centro de Investigacion en Ciencia Aplicada y Tecnologia Avanzada del I.P.N, Unidad Queretaro, Queretaro, México.
[z] E-mail: mario@mie.utoronto.ca

Downloaded 21 Jul 2008 to 128.100.49.17. Redistribution subject to ECS license or copyright; see http://www.ecsdl.org/terms_use.jsp

S0013-4651(99)05-082-X CCC: $7.00 © The Electrochemical Society, Inc.

Hankel transform $N(z, \lambda; \omega)$ of the three-dimensional free carrier density $N(\mathbf{r}, \omega)$ by integrating over the thickness of the wafer, which takes into account deep-lying Plank radiation emission from photogenerated and diffused carriers, according to Kirchhoff's law of detailed balance.[3] The result for the plasma contribution in Hankel space (λ) is

$$F(\lambda,\omega)=\int_0^L N(z,\lambda;\omega)dz=\frac{e^{-\lambda^2 d^2/8}}{(D_n b_n+S_1)b_n}\left(\frac{A_2+e^{-b_n L}}{A_2-A_1 e^{-2b_n L}}\right) \quad [3]$$

The parameters in Eq. 3 are defined as follows

$$b_n^2=\lambda^2+\sigma_n^2$$
$$A_1=\frac{D_n b_n-S_1}{D_n b_n+S_1} \quad [4]$$
$$A_2=\frac{D_n b_n+S_2}{D_n b_n-S_2}$$

where d is the laser beam spot size and $\sigma_n^2=(1+i\omega\tau_n)/D_n\tau_n$. The other parameters are as defined earlier. The thermal component is calculated in the same manner

$$T(\lambda,\omega)=B_1\left(\frac{1-e^{-b_t L}}{b_t}\right)+B_2\left(\frac{e^{b_t L}-1}{b_t}\right)+B_3\left(\frac{1-e^{-b_n L}}{b_n}\right)+B_4\left(\frac{1-e^{-b_n L}}{b_n}\right)e^{-b_n L} \quad [5]$$

The parameters in the above equation are defined as follows

$$B_1=\frac{h_1-h_2 e^{-b_t L}}{1-e^{-2b_t L}}$$
$$B_2=\left(\frac{h_1 e^{-b_t L}-h_2}{1-e^{-2b_t L}}\right)e^{-b_t L}$$
$$B_3=\frac{E_g e^{-\lambda^2 d^2/8}}{\pi h\upsilon k\tau_n\left(b_n^2-b_t^2\right)\left(D_n b_n-S_1\right)}\left(\frac{A_2}{A_2-A_1 e^{-2b_n L}}\right)$$
$$B_4=B_3\left(\frac{A_1}{A_2}\right) \quad [6]$$
$$h_1=\frac{-S_1\tau_n}{b_t}\left(b_n^2-b_t^2\right)\left(B_3+B_4 e^{-2b_n L}\right)-\frac{b_n}{b_t}\left(B_3-B_4 e^{-2b_n L}\right)$$
$$h_2=\frac{1}{b_t}\left[S_2\tau_n\left(b_n^2-b_t^2\right)\left(B_3+B_4\right)\right]-b_n\left(B_3-B_4\right)e^{-2b_n L}$$
$$b_t^2=\lambda^2+\sigma_t^2$$

where $\sigma_t^2=i\omega/\alpha$. This three-dimensional PTR model takes into account the finite size of the exciting Ar^+ ion laser beam and the Si absorption depth at the wavelength 514.5 nm; the effective detector size, and the sample thickness.[6] Before examining the PTR measurements within the framework of our 3D theory, it is necessary to understand the influence of all the input parameters in shaping the frequency response according to the model.

To examine the influence of these carrier and thermal transport parameters, a procedure that consists of varying each of the aforementioned parameters τ, $D_{n,p}$, S_1, S_2, C_t, C_p while keeping the remaining parameters constant, is presented. Depending on the value of the recombination lifetime, each parameter has a different influence on the PTR signal for the examined frequency range 10 Hz to 100 kHz, and this is valuable information toward the uniqueness aspects of our theory to experimental data.

Recombination lifetime simulations.—The carrier lifetime in silicon can be referred to as minority carrier recombination lifetime (τ_o) only under rather restrictive conditions: (*i*) very low injection level; (*ii*) the doping density in the sample is less than that required for the onset of degeneracy $\sim 10^{19}$ atom/cm^3 [7]; and (*iii*) the defect centers lie far enough from the bandedges.[7,8] In order to clarify the effect of the injection level in our experimental results, we carried out two different experiments. First we examined the relationship between PTR amplitude and laser power for low frequency values using neutral filters. We found a linear relation between them in the range from 5 to 75 mW with no change in the shape of the frequency curve. As a second step, a frequency scan was carried out for three laser intensities (50, 15, and 7 mW) on the sample. After the foregoing experimental data were fitted to the theory, we found the same electronic properties. Therefore, these measurements imply that the electronic transport parameters remained unchanged as power increased and can be taken as a criterion for an effective low-level injection. It is well known that τ_o reflects the properties of the defect centers in a given Si substrate. It is usually very difficult, however, to identify the particular impurity that controls the lifetime. Some examples are iron in boron-doped silicon (p-Si)[8] and in low doped n-silicon.[11,12] Iron atoms can be reversibly cycled between two different electrically active defect centers, and the combination of these defect centers results in a unique recombination lifetime signature. Further studies show that different recombination centers are responsible for the magnitude of the recombination lifetime in doped silicon[9,11] and in thin silicon epitaxial layers.[10]

Effective criteria for the uniqueness of the fitting parameters stem from the requirement that they have to be reasonably close to the reported values in the literature for Si, Table I. These values are used as "seeds" for the multiparameter searches. Figure 1 shows a recombination lifetime simulation and the effects of changing τ on the PTR signal amplitude (a) and phase (b), assuming the following parameters: $S_1 = 130$ cm/s, $S_2 = 1.6 \times 10^6$ cm/s, $\alpha = 0.116$ cm^2/s, $D_n = 5$ cm^2/s, $C_p = 3 \times 10^{-20}$ arbitrary units (a.u.), and $C_t = 1$ a.u. The chosen values of the parameters (S_1, S_2, α, D_n) are within the range of values reported in the literature for p- and n-silicon; see Table I. For these and all subsequent simulations, a wafer thickness of 670 μm was used. In our simulations, the value of the recombination lifetime, τ, was varied between 10 and 5,000 μs. For each τ value, both amplitude and phase exhibit a characteristic bend (knee) that shifts to higher frequencies as the lifetime decreases. An important feature of the amplitude curves is that when the lifetime increases, the PTR signal amplitude also increases and the characteristic knee shifts parallel to the frequency axis toward lower frequencies. The amplitude levels off at low frequencies, with the saturation level clearly dependent on the value of τ. This is due to the fact that longer recombination lifetimes result in higher free-carrier density contributions to the depth integrals, to which the PTR signal is proportional. The main conclusions with respect to this simulation are (*i*) that the value of the recombination lifetime determines the departure of both amplitude and phase levels from their low-frequency saturation, and thus determines the position of the downward "knees" in Fig. 1. The frequency position, f_c, of the "knee" is also subject to the simple mathematical relationship[3] $2\pi f_c\tau \sim 1$ related to the characteristic lifetime τ. Therefore, the lifetime values found in the fitting procedure have to be close to the value given by this relationship; and (*ii*) the low-frequency saturation-level of the amplitude curve increases in proportion to increasing lifetime and eventually saturates for $\tau > 5$ ms. The sensitivity of the PTR signal decreases when the lifetime increases. In practice, the available frequency bandwidth of PTR, 1 Hz–100 kHz, allows the measurement of lifetimes in the range $\sim$10 ms to $\sim$1 μs. This range is very satisfactory for today's Si wafer technologies.

Plasma-and-thermal coefficient simulations.—Owing to the pervasive influence of the recombination lifetime across the modulation frequency spectrum, further simulations with respect to the remaining transport parameters were separated into two different groups of

Downloaded 21 Jul 2008 to 128.100.49.17. Redistribution subject to ECS license or copyright; see http://www.ecsdl.org/terms_use.jsp

S0013-4651(99)05-082-X CCC: $7.00 © The Electrochemical Society, Inc.

Table I. Reported literature values for thermal and electronic parameters of Si wafers.

Type	α (cm^2/s)	$D_{n,p}$ (cm^2/s)	S_1 (cm/s)	S_2 (cm/s)	τ (μs)	Front surface state	Back surface state	Technique	Annealing	Ref.
p	0.80	30	100		10.5	Polished		PTR 1-D	Thermal	16
p	0.80	30	750		1-10			TW-PTR	P implant	16
p	0.85	18.3	331.6			Polished	Rough	PAS		15
p	1.03	34.1	334.6	334.6		Rough	Rough	PAS		15
p		34.5[a]	10^4			Polished				8
p			0.25			Polished			Chemical	19,20
p			20			Polished			thermal	20
p			$<10^4$			Polished			Thermal	21
p			3600			Polished			Thermal	21
p		35,5	70						Thermal	17
p		35.5	$2\text{-}3\cdot10^3$			As sliced				17
p		35.5	20		10^3				Chemical	17
p		33-36.4	$1\text{-}10^3$	$1\text{-}10^3$		Polished	Polished	PCD	Thermal	22
p		33-37	1	10^7		Polished	Abraded	PCD	Thermal	22
p			10^7	10^7		Abraded	Abraded	PCD	Plasma etching	22
p		40[a]	110			Polished			Thermal	23,24
p			410	Infinite	17.7			PTR 1-D		1
p			410		17.7			PTR 3-D		1
p		33[a]		10^5	330			SPV		25
n			$10^2\text{-}10^5$			Polished			Thermal	18
n			$2\cdot10^5\text{-}3\cdot10^6$			Bare	Bare	PCD		18
n		10	320-830	$1.6.10^5$	320	Bare/Polished	As sliced	PTR		4
N		15.9[a]				Polished				8
N	0.96	10	328-830		110		Polished	3D-PTR		14
N		12.5	$2\text{-}3\cdot10^3$			As sliced				17
N		12.5	3		10^4			PCD	Chemical	17
N		12.5	15						Thermal	17
N		12[a]		10^5	500			SPV		25
N					40	As sliced		LMPC		27
N					10^3	Polished	Polished	LMPC	Thermal	27

[a] Assumed
PAS: photoacoustic spectroscopy
TW: thermal wave
3D-PTR: photothermal radiometry
1D-PTR: photothermal radiometry
PCD: photoconductance decay
SPV: surface photovoltage
LMPC: laser/microwave photoconductance

p-type Si wafers: samples with long lifetime (LL), and samples with short lifetime (SL). Each group consisted of several values of the remaining parameters: D_n (p-Si), S_1, S_2, and various contributions of the plasma and thermal components. Simulations of the thermal component contribution to the PTR signal amplitude (a) and phase (b) are shown in Fig. 2 with the following parameters: S_1 = 130 cm/s, $S_2 = 1.6 \times 10^6$ cm/s, $\alpha = 0.116$ cm^2/s, $D_n = 5$ cm^2/s, $C_p = 3 \times 10^{-20}$ a.u. Both long-lifetime (LL) and short-lifetime (SL) groups of curves are shown in this figure. When the PTR signal is dominated by the thermal coefficient ($C_t > 3$ a.u.) at low frequencies in silicon with long lifetime, Fig. 2a, there is a characteristic nonzero slope (<100 Hz) in both phase (downward trend) and amplitude (upward trend). The effects of C_t are entirely confined to the low frequency region. The phase *lag* is largest for samples with long lifetime, as expected from the slow thermal conduction mechanism to the front surface, following carrier diffusion away from the photoinjection spot, and recombination deep inside the bulk of the Si wafer. This effect is much more diminished in SL silicon, because most free carriers de-excite close to the surface and only a small phase lag is possible. At values $C_t < 3$ a.u. the photogenerated plasma-wave emission dominates the PTR signal even at the lowest frequencies. Both amplitude and phase become essentially flat, Fig. 2a,b. The phase is essentially zero at $f < 100$ Hz, because the relatively fast plasma-wave photogeneration rate modulates the PTR signal response in-phase with the laser beam modulating optical waveform.[3,13] The main conclusion of this computational simulation is that, if the experimental data do not exhibit the characteristic low-frequency (amplitude and phase) nonzero slope, the signal is dominated entirely by the plasma component, regardless of the lifetime value, which, in any case, is short compared to the modulation period $T = 1/f$.. Conversely, the presence of a nonzero low-frequency slope is an indicator of strong thermal response and can be used to determine the bulk thermal diffusivity of the electronic material.

Minority carrier diffusion coefficient simulations.—The PTR signal amplitude and phase for a Si sample with short lifetime (τ = 100 μs), with the minority carrier diffusion coefficient (D_n) as a parameter are shown in Fig. 3a and b, respectively. The diffusion coefficient measures the electronic diffusion of minority carriers throughout the sample, away from the photogeneration point under the laser-illuminated spot. D_n (D_p) represents an important quality factor for device fabrication on a given wafer as a means of determining the device-relevant electronic diffusion length. The following relation between the lifetime and the carrier diffusion coefficient defines the diffusion length L

$$L = \sqrt{D_n \tau} \qquad [7]$$

According to Eq. 7, the carrier diffusion length, L, may be smaller than the thickness of the wafer, in which case the diffusing minority carriers cannot reach the opposite surface of the sample. Also L may be larger than the wafer thickness, in which case the minority carriers can reach, and possibly recombine nonradiatively at, the back

Downloaded 21 Jul 2008 to 128.100.49.17. Redistribution subject to ECS license or copyright; see http://www.ecsdl.org/terms_use.jsp

S0013-4651(99)05-082-X CCC: $7.00 © The Electrochemical Society, Inc.

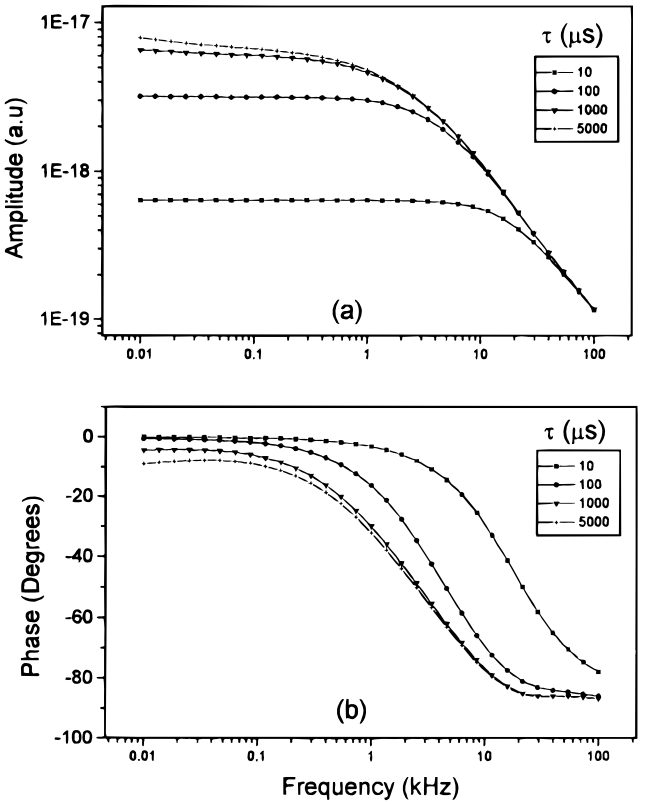

Figure 1. PTR signal amplitude (a) and phase (b) for lifetime simulations in Si samples. Values uses for these simulations were: $D_n = 5$ cm^2/s, $S_1 = 130$ cm/s, $S_2 = 1 \times 10^4$ cm/s, $\alpha = 0.116$ cm^2/s, $C_p = 3 \times 10^{-20}$ a.u, $C_t = 1$ a.u.

surface, thus generating an additional thermal wave source. The PTR signal amplitude in Fig. 3a increases monotonically with decreasing D_n at low frequencies (<10 kHz). Similar effects are observed with long-lifetime Si wafers, Fig. 1a. A decrease of the diffusion coefficient further shifts the characteristic knee to lower frequencies. The amplitude- and phase-frequency response curves eventually saturate at very high D_n. This trend occurs because lower diffusion coefficients amount to higher probability of carriers to remain within the PTR signal detection volume until they recombine radiatively or nonradiatively. This volume is centered about the laser spot size that has an effective area of πa_{max}^2 and a thickness approximately equal to the optical absorption depth, β^{-1}, at the excitation wavelength or the *ac* carrier diffusion length, $L_n(\omega) = (D_n\tau)^{1/2}/(1 + i\omega\tau)$. Here, a_{max} is the IR detector equivalent radius (imaged on the surface of the wafer), or the laser-beam spot size, w, whichever is greater. $\beta(\lambda)$ is the optical absorption coefficient of Si. De-exciting carriers in traps within the bandgap are "counted" by the PTR detector as they decay locally, by emitting Planck radiation which is captured by the IR optics.[3] Both the amplitude and phase simulations show that the effect of decreasing D_n is similar to increasing lifetime, in the sense that the free carrier density increases under the probe. The effect of diffusion coefficient value variations on the PTR amplitude, Fig. 3a, is similar to varying the lifetime. The effect on the PTR phase, however, is different in the low frequency region, Fig. 3b. Thus, for a simultaneous theoretical fit to both signal channels, amplitude and phase, the variations of lifetime value and diffusion coefficient value manifest themselves quite differently, a fact which assures the uniqueness of the fit with respect to these parameters. Higher D_n values lead to higher-frequency bends, the actual amplitude level and slope of which eventually saturate above a certain frequency. This occurs because at low frequencies and small D_n, the number density of carriers decaying (counted) within the probe region of the IR detector is controlled by the lifetime, and so is the frequency posi-

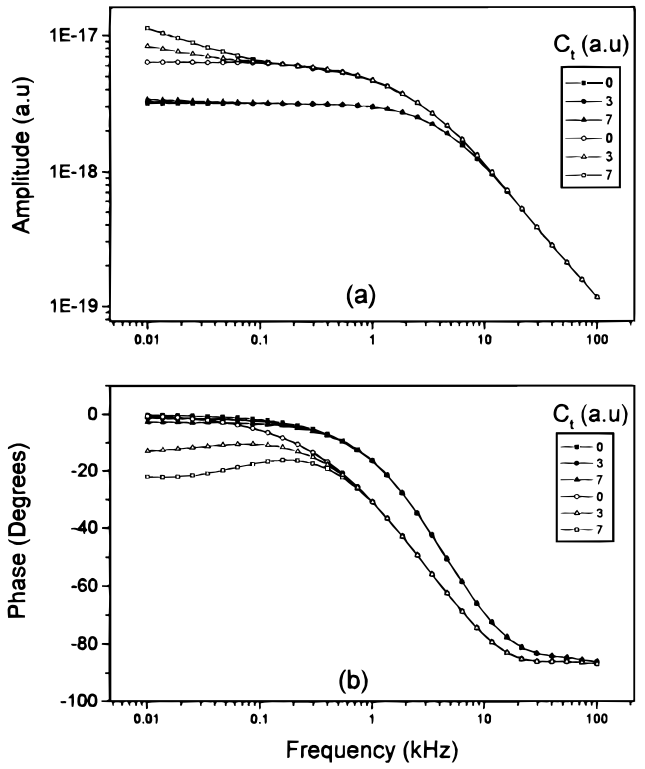

Figure 2. PTR signal amplitude (a) and phase (b) for plasma and thermal component simulations in p-Si samples with long lifetime (LL, open) and short lifetime (SL, full). Values used for these simulations were (LL = 1500 μs, SL = 100 μs, $D_n = 5$ cm^2/s, $S_1 = 130$ cm/s, $S_2 = 1 \times 10^4$ cm/s, $\alpha = 0.116$ cm^2/s, $C_p = 3 \times 10^{-20}$ a.u.

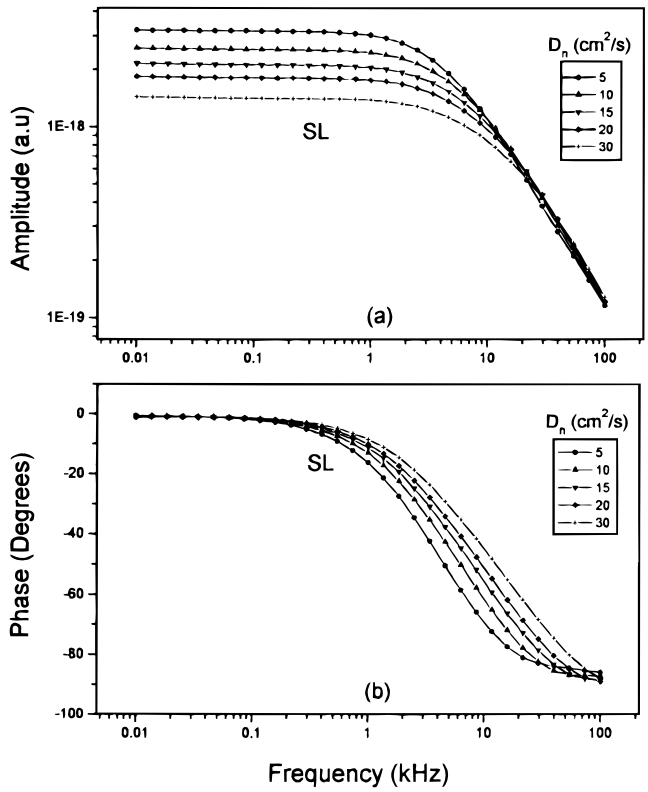

Figure 3. PTR signal amplitude (a) and phase (b) for carrier diffusion coefficient simulations in Si samples with short lifetime ($\tau = 100$ μs). Values for the remaining simulation parameters were $D_n = 5$ cm^2/s, $S_1 = 130$ cm/s, $S_2 = 1 \times 10^4$ cm/s, $\alpha = 0.76$ cm^2/s, $C_p = 3 \times 10^{-20}$ a.u and $C_t = 1$ a.u.

Downloaded 21 Jul 2008 to 128.100.49.17. Redistribution subject to ECS license or copyright; see http://www.ecsdl.org/terms_use.jsp

S0013-4651(99)05-082-X CCC: $7.00 © The Electrochemical Society, Inc.

tion of the bend, as in Fig. 3. For large D_n values, however, the free carrier density is controlled by the relative sizes of the IR detector equivalent radius, *a*, and by the ac diffusion length $L_n(\omega)$. If $L_n(\omega) > a$, (low frequencies), the rate of carrier transfer out of the detector imaging area increases as L_n increases with higher D_n. This results in decreasing the PTR signal amplitude due to uncounted carriers leaving the viewing region. The bend appears when the $L_n(\omega)$ shrinks enough at high frequencies to become smaller than *r*, toward a saturation value for $|L_n| << a$. In this case, the lifetime becomes, once again, the determining factor for the slope of the curve, because it serves as a mechanism for storing optical energy in the excited electronic state. In the simulation of Fig. 3a the slope saturates because a common lifetime has been assumed for all the curves. Of course, by virtue of the structure of the $L_n(\omega)$ dependence on D_n and on ω, the larger the value of D_n, the higher the frequencies where the condition $|L_n(\omega)| \sim a$ holds. The influence of the lifetime value on D_n simulations can be appreciated in the low frequency region: the amplitude level and amplitude spread (between signals with lowest and highest D_n) are found to be larger for longer lifetimes.

Front surface recombination velocity.—PTR amplitude and phase simulations for Si samples (1500 μs) with the front surface recombination velocity (S_1) as a parameter are shown in Fig. 4a and b, respectively. This phenomenological parameter is a measure of the electronic quality of the front surface in terms of the structure and density of traps and surface states acting as recombination sites. For both long- and short-lifetime samples, the amplitude exhibits a strong dependence on S_1, decreasing dramatically with increasing S_1. This is due to the efficient thermal conversion on the surface, which depletes the free-carrier density there. S_1 has a much weaker effect, however, on the PTR phase at very low frequencies (<0.1 kHz) because the thermal-conversion source is located at near-surface depths too short compared to the shortest thermal or carrier diffusion length. The phase response is sensitive to S_1 at high frequencies through a shift of the centroid of the carrier-density depth distribution closer to the surface (smaller lag) with increasing S_1. Barring recombination at, or near, the surface, the phase lag is normally controlled by the speed of the carrier-density centroid's diffusion into the bulk of the wafer. This characteristic high-frequency phase response is used in multiparameter fits to uniquely determine the value of this parameter.

Back-surface recombination velocity.—The effects of the value of the back surface recombination velocity, S_2, for a Si sample with long lifetime are shown in Fig. 5. This parameter has a weak influence on the amplitude and phase of the PTR signal, and only in the low frequency range (<0.1 kHz) and for very large values of S_2 (>10^6 cm/s). Such values are normally not encountered with industrial quality Si-polished wafers. For samples with short lifetimes, the effect of this parameter is not significant either. This is expected, since the ac carrier diffusion length, $L(\omega)$, is short compared to the sample thickness for all values of the modulation frequency. Figure 5 shows that the PTR signal amplitude increases with increasing S_2. This occurs due to the increase in the thermal-wave component of the signal (characterized by the nonzero slope), in the thermally thin material at low frequencies. For low values of S_2 the phase saturates to zero at low frequencies as expected from a dominant carrier plasma wave. For values smaller than 10^6 cm/s the effect is negligible. The phase lag increases as the value of S_2 increases. Conversion of excited-state, free-plasma-stored energy to thermal-wave at the back surface, and diffusion of heat toward the front surface, shifts the signal-generation centroid to increasingly deeper coordinate points inside the bulk of the wafer.

A summary of the influence of the various parameters on the amplitude and phase of the PTR signal of a typical Si wafer is shown in Table II, which includes a comment column on the sensitivity of the PTR technique to each parameter. Low frequency (<1 kHz) and

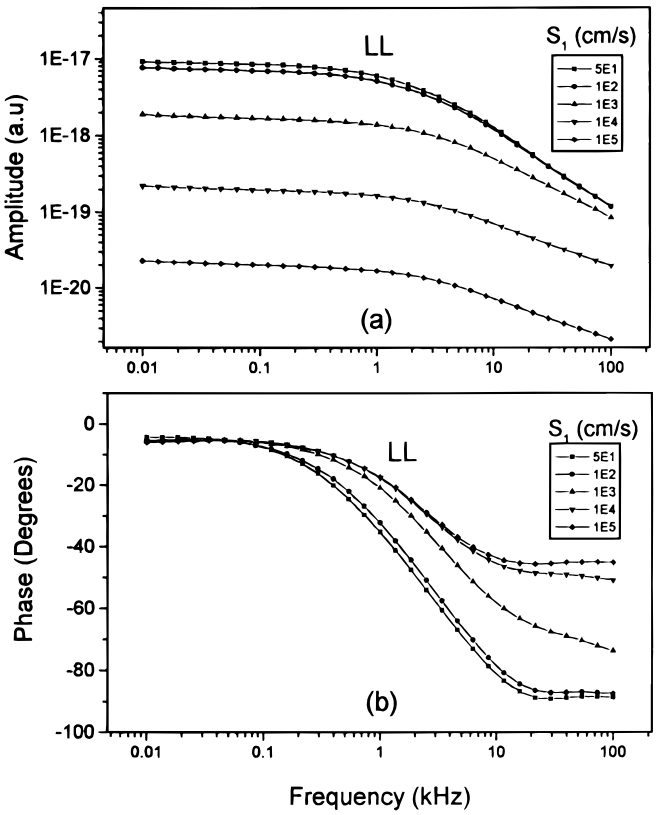

Figure 4. PTR signal amplitude (a) and phase (b) for front surface recombination velocity simulations in Si samples with long lifetime (τ = 1500 μs). Values for the remaining simulation parameters were $D_n = 5$ cm^2/s, $S_2 = 1 \times 10^4$ cm/s, $\alpha = 0.116$ cm^2/s, $C_p = 3 \times 10^{-20}$ a.u, and $C_t = 1$ a.u.

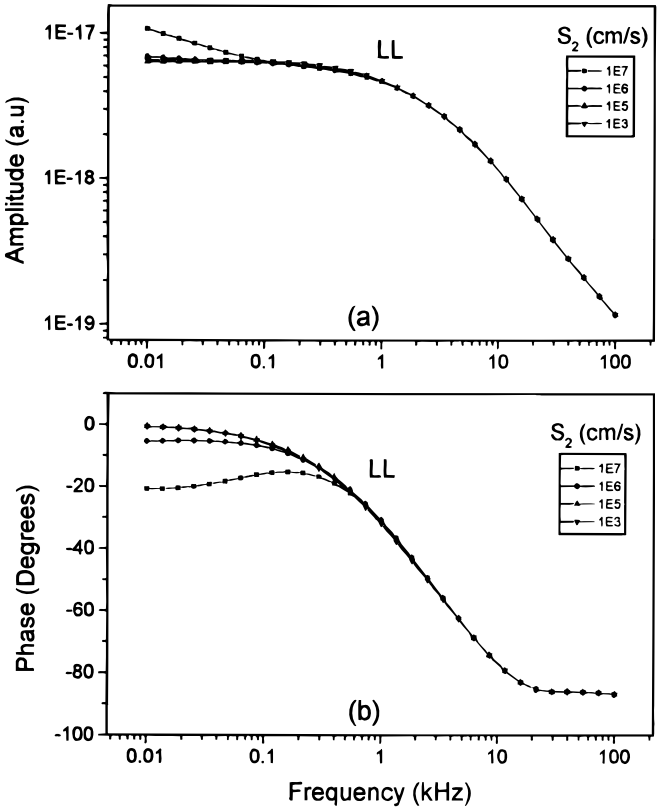

Figure 5. PTR signal amplitude (a) and phase (b) for back surface recombination velocity in Si samples with long lifetime (τ = 1500 μs). Values for the remaining simulations parameter were $D_n = 5$ cm^2/s, $S_1 = 130$ cm/s, $\alpha = 0.116$ cm^2/s, $C_p = 3 \times 10^{-20}$ a.u, and $C_t = 1$ a.u.

Downloaded 21 Jul 2008 to 128.100.49.17. Redistribution subject to ECS license or copyright; see http://www.ecsdl.org/terms_use.jsp

S0013-4651(99)05-082-X CCC: $7.00 © The Electrochemical Society, Inc.

Table II. General trends for PTR parameters as a function of modulation frequency for p-Si samples with short and long lifetime.

Parameter	PTR Signal	Effect on signal LowFrequency (≈ <1 kHz)	Effect on signal High Frequency (≈ <1 kHz)	Ref. figures	Comments on sensitivity
$\tau\uparrow\downarrow$	Amp. Phase	A↑↓, moderate φ↓↑, strong	A↑↓, moderate φ↓↑, strong	Fig. 1a and b	Sensitivity decreases with increasing carrier lifetime
$D_n\uparrow\downarrow$	Amp., τ_{LL} Phase, τ_{LL} Amp., τ_{SL} Phase, τ_{SL}	A↓↑, strong φ↑↓, weak A↓↑, strong φ↑↓, weak	A↑↓, strong φ↑↓, strong A↑↓, weak φ↑↓, strong	Fig. 3a and b	High sensitivity for both LL and SL samples
$S_1\uparrow\downarrow$	Amp., τ_{LL} Phase, τ_{LL} Amp., τ_{SL} Phase, τ_{SL}	A↓↑, strong φ↑↓, (0.1~1kHz) moderate A↓↑, strong φ↓↑,((0.1kHz) moderate	A↓↑, strong φ↑↓, strong A↓↑, strong φ↑↓, strong	Fig. 4a and b	High sensitivity for both LL and SL samples
$S_2\uparrow\downarrow$	Amp. τ_{LL} Phase τ_{LL} Amp. τ_{SL} Phase τ_{SL}	A↑↓, weak φ↓↑, moderate A↑↓, weak φ↓↑, weak	No effect No effect No effect No effect	Fig. 5a and b	Very low sensitivity for LL samples and no sensitivity for SL samples
$C_t\uparrow\downarrow$	Amp. τ_{LL} Phase τ_{LL} Amp. τ_{SL} Phase τ_{SL}	A↑↓, moderate φ↓↑, strong (0.01~0.1kHz) A↑↓, weak φ↓↑, weak	No effect No effect No effect No effect	Fig. 2a and b	

Key to arrow signs:

	Amp.	Phase φ
↑	Increase	Less negative
↓	Decrease	More negative

τ_{LL}: long lifetime; τ_{SL}: short lifetime.

high frequency (>1 kHz) regions are shown separately (columns 3 and 4 from left-to-right, respectively). The 1 kHz frequency is (roughly) considered as the transition from the thermal-wave to the plasma-wave dominating mechanism in typical industrial quality Si samples, such as those investigated in this work. Recombination lifetime has strong influence across the entire frequency range. The parameters C_t and S_2, have a weak-to-moderate (short lifetime) and moderate-to-strong (long lifetime) effect on the PTR signal at low frequencies only. The carrier diffusion coefficient has a moderate-to-strong effect in the low frequency range and a weak (amplitude) to strong (phase) effect at high frequencies. The effect of S_1 on the PTR signal (amplitude and phase) is strong at high frequencies and weak-to-moderate at low frequencies. The particular (characteristic) influence of each parameter on the PTR signal is a means for obtaining a unique set of parameters for a particular Si sample. In order to establish a methodology for obtaining a unique multiparameter fit, a fitting procedure based on Eq. 2 through 6 is described below as applied to amplitude and phase data obtained from PTR measurements on three industrial Si wafers.

Experimental

The experimental arrangement of our PTR instrument for Si wafer diagnostics is shown in Fig. 6. An argon-ion (514.5 nm) laser beam was passed though an acousto-optic modulator (AOM) and a beam expander (10 times) producing a 1 cm beam size. The expanded beam was then focused onto the sample surface by using a gradium glass lens of 12.4 cm focal distance. The spot size of the focused laser Gaussian beam was approximately 48 μm in diam. PTR results using this spot size require a three-dimensional signal analysis owing to the radial degrees of freedom for energy and/or carrier diffusion.[4,6,14] The beam size was estimated by Gaussian fitting of the laser beam with a beam profilometer (Spiricon LBA-100A V3.03). The optical power incident on the sample was typically between 20 and 50 mW, thus satisfying effective low-injection conditions, as discussed above. When the reflectivity of Si at 514.5 nm for normally incident beam (~0.4) [26] is taken into account, it is seen that it further reinforces the low-injection limit conditions. The resulting diffuse infrared blackbody radiation emitted from the semiconductor surface was collected, collimated, and focused by two off-axis paraboloidal mirrors. The signal was detected by a liquid-nitrogen-cooled photoconductive mercury-cadmium-telluride (MCT) IR detector with spectral response between 2 and 12 μm. The output signal from the MCT was preamplified and fed to a lock-in amplifier,

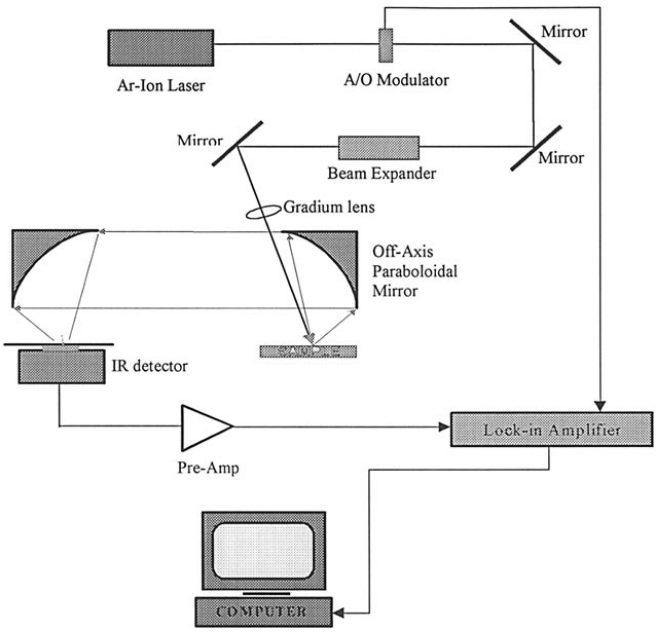

Figure 6. Experimental setup for 3-D PTR semiconductor metrology.

Downloaded 21 Jul 2008 to 128.100.49.17. Redistribution subject to ECS license or copyright; see http://www.ecsdl.org/terms_use.jsp

S0013-4651(99)05-082-X CCC: $7.00 © The Electrochemical Society, Inc.

which demodulates the generated diffusion-wave signal. To obtain the electronic parameters of a Si wafer, a frequency scan typically in the range between 10 Hz to 100 kHz is required. In the reported measurements, data acquisition, and control of the frequency scan were performed using a personal computer. All the experimental measurements were normalized by the instrumental transfer function obtained from a protocol using two reference samples: a zirconium alloy (pure thermal contribution), followed by further normalization with the PTR signal from a high-quality Si wafer with purely electronic behavior. The second normalization was necessary in order to eliminate thermal-wave noise from the Zr reference at high frequencies, which tended to degrade the superior signal-to-noise ratio of the electronic response of typical Si wafers.

Three thermally oxidized samples 15 cm (6 in.) in diameter, of p-type silicon wafers supplied by Mitel Semiconductors (Bromont, Quebec), were examined using the PTR method. Two of these wafers (no. 5 and no. 6) had a center-point resistivity between 14 and 24 Ω-cm ("low resistivity" wafers). The other wafer (no. 30) had a center point resistivity between 25 and 44 Ω-cm ("high resistivity" wafer). These wafers contained center-point oxygen concentration between 24 to 32 ppma and carbon concentration of 0.5×10^{17} atom/cm^3. These wafers were part of a broader study of as-received industrial Mitel wafers for PTR diagnostics.

Thermal dry isochronal annealing was carried out using a horizontal furnace BDF-200. A side cross sectional view of this furnace is shown in Fig. 7. The gas inlet was located at the back of the furnace ("source") and the gas exit was located at the opposite end of the furnace ("door"). Inside the tube there was a negative static pressure of 0.3 psi to evacuate the gas. The system was, nevertheless, considered to be under STP conditions, without vacuum. The polished side of the wafers was facing the door. Thus, the gas was flowing toward the back of the wafers. Each tube could accommodate four quartz boats and each boat could hold 25 wafers. Wafers no. 5, 6, and 30 were used for front and back surface measurements, as well as for radial and surface radiometric imaging scans. Wafers no. 5 and 30 were located in the first quartz boat near the furnace door, Fig. 7. Wafer no. 6 was located in the first quartz boat near the furnace source, Fig. 7. The spacing between two adjacent wafers was 3 mm. The tube was surrounded by heating elements, which provided uniform temperature distribution across its length. All wafers were subjected to the following thermal cycle: they were first exposed to 800°C for 10 min. After reaching thermal equilibrium, the wafer temperature was ramped-up from 800 to 1175°C under low flows of O_2 and N_2 gases for 40 min, at a rate of 5°C/min. The temperature was stabilized at 1175°C and dry oxidation was induced in pure O_2 for 6 h, 50 min. At the end of the oxidation process, the furnace temperature was ramped-down to 800°C in pure N_2 at a rate of 5°C/min. The grown oxide thickness was 4570 Å. Both surfaces of the wafers used in this work were exposed to the same gas flow and temperature conditions, under the isochronal dry oxidation process. Therefore, they were expected to exhibit similar surface recombination velocities, even if the front surface had been polished chemically and mechanically. PTR diagnostics of both surfaces of several wafers were performed and the results on the foregoing three wafers are discussed in the following section.

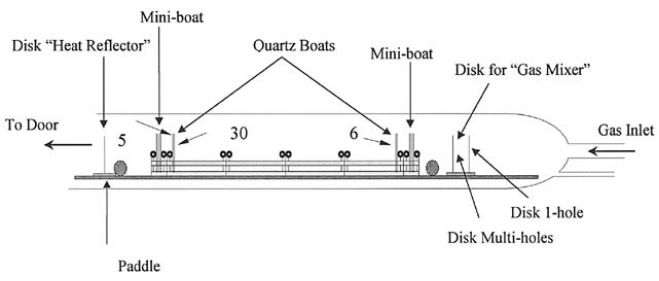

Figure 7. Schematic representation of the horizontal furnace used for dry isochronal oxidation process.

Computational Methodology and Multiparameter Fits

In order to obtain a particular set of parameters from PTR measurements of a Si wafer, a multiparameter fitting procedure based on the simulation trends explored in the previous sections was developed. The methodology was applied to two samples, a high resistivity (wafer no. 30) and a low resistivity sample (wafer no. 5). Both wafers were thermally annealed and had a polished front surface and a rough (matte) back surface. The computational best-fit procedure includes the following steps: (*i*) selection of initial values within the range of the physical parameters reported in the literature (see Table I); (*ii*) variation of the thermal and plasma coefficients (C_t and C_p), until a good fit is obtained at the low-frequency range of both experimental phase and amplitude; (*iii*) variation of the recombination lifetime value, until the characteristic knee of the experimental curve is best-fitted and is consistent with the $2\pi f_c\tau \sim 1$ criterion. These procedures are then followed by readjusting the thermal and plasma coefficients to match phase and amplitude at the low frequency range; (*iv*) variation of D_n until the intermediate region of the phase and the amplitude signal converge to the experimental data. Then phase and amplitude are adjusted while C_t and C_p are also varied, as required; (*v*) variation of S_1, until the signal phase spread between the two frequency range extremes (10 Hz to 100 kHz) is matched to the experimental spread. Since the amplitude is also affected by this parameter, this procedure is followed by a readjustment of the amplitude at low frequencies by varying C_t and C_p, as required; (*vi*) variation of the back-surface recombination velocity, S_2, for fine-tuning at low frequencies, only when the data are sensitive to S_2. This is followed by a readjustment of both phase and amplitude at low frequencies by varying C_t and C_p, if necessary; and (*vii*) fine-tuning of the fit by repeating steps *iii* to *vi*.

It is well known that lifetime values vary across a silicon wafer.[11] This has also been observed with the present PTR experiments. However, this variation has a special significance in the case of PTR amplitude measurements. When multipoint measurements across the surface of a single sample are performed, an extra channel of information is available, that is the relative positions of the flat (low-frequency) region of the amplitude curves scale linearly with lifetime at a given point, Fig. 1 and 11. The relative values of the amplitude with respect to other locations further reinforce the consistency of the foregoing computational procedure by cross-correlation of the measured lifetimes. Based on Fig. 11, amplitude scans can immediately yield lifetime maps upon calibration, as in the case of Fig. 12 below.

As discussed earlier on, for a reliable and unique multiparameter fit it was found very helpful to establish realistic initial "seed" values for the various electronic parameters based on the literature summary shown in Table I. The thermal diffusivity is a bulk property and our simulations indicated that it has a weak influence in the PTR signal (both amplitude and phase). The values chosen for these simulations were 0.75 and 0.96 cm^2/s for low and high resistivity, respectively. These values are in close agreement with those reported in the literature.[15,16] The range of values reported in the literature for the front surface recombination velocity of n- and p-silicon is between 0.25 cm/s, for a very passivated surface, and 10^7 cm/s for highly doped p-silicon (Table I). A low value of the front surface recombination velocity (*i.e.*, 100 cm/s) for a p-silicon, which represents a moderately passivated surface, was chosen as our initial value. For the Si wafers of this study, the back surface was subjected to the same thermal process as the front surface. Therefore, the S_2 value of 100 cm/s, the same as S_1, was chosen to initialize the fitting procedure. Initial relative values for C_t and C_p were 1 and 3×10^{-20} a.u, respectively. The reported values for $D_{n,p}$ are in the range between 8 and 36.4 cm^2/s (Table I, column. 3). We chose 7.5 cm^2/s (the lower limit) as the initial value for our fitting procedure. Finally, to start the fitting procedure, a value of 1500 and 100 μs were chosen for minority carrier lifetime of high and low resistivity wafers, respectively. Once the initial values were chosen, the cyclic fitting procedure with the feedback described above was followed, steps *i* to *vii*. This procedure was performed manually in an electronic sheet program. The implementation of an automated computer program for the sequential cyclic multiparameter fitting procedure is currently under way.

Downloaded 21 Jul 2008 to 128.100.49.17. Redistribution subject to ECS license or copyright; see http://www.ecsdl.org/terms_use.jsp

S0013-4651(99)05-082-X CCC: $7.00 © The Electrochemical Society, Inc.

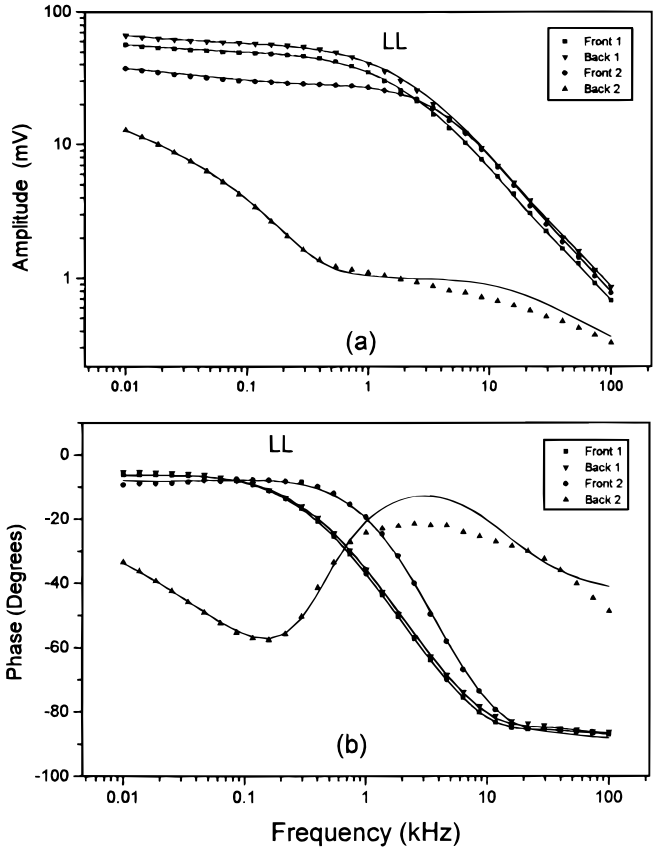

Figure 8. PTR signal amplitude (a) and phase for a Si sample with long-lifetime wafer no. 30, before (front 1 and back 1) and after (front 2 and back 2) damage, respectively.

Multiparameter Best-Fit Results from Intact and Damaged Wafers

Front- and back-surface PTR measurements.—Frequency scans were performed at the center point of the two test wafers, high resistivity wafer no. 30 and low resistivity wafer no. 6, with the laser beam impinging successively on the front surface and on the corresponding spot of the back surface. Then, small spots on the back surface of the wafers were intentionally scratched, and the frequency scan was repeated. Silicon carbide paper with an average particle size of 22 μm was used to scratch the surface. After roughening the back surface, effects due to changes in the surface recombination velocities were expected as indicated in Fig. 4 and 5. The experimental PTR signal for a Si sample with long lifetime (sample no. 30) obtained from these frequency scans are shown in Fig. 8. The solid squares and inverted triangles represent frequency scans for both surfaces prior to damaging the back surface. The experimental amplitude and phase curves are almost identical indicating similar electronic transport parameters in both directions. The solid lines represent the best fits to the experimental data following the aforementioned procedure. The measured values of the various parameters for the front and back surface before (front 1 and back 1), and after (front 2 and back 2), scratching the back surface are shown in Table III. The fitting values obtained for S_2 (1000 cm/s) were in the nonsensitive region according to the simulations discussed previously (see Fig. 4). Therefore no conclusions regarding this parameter could be made. The electronic parameters obtained for the front and back surface (before scratching) were similar except that S_1 was slightly higher. These results indicate that the dry oxidation process did, indeed, have the same effect on both surfaces. The solid circles and solid upright triangles represent the frequency scans after the damage on the back surface. The PTR amplitude, in the high frequency range, of the front-surface signal (front 2) in the case with the damaged region is similar to that obtained from the case with the intact wafer surface (front 1). However, there are significant changes regarding the PTR signal obtained from the back surface (back 1) and the damaged region case (back 2). In Table III, the value of τ for the scratched back surface represents an average recombination lifetime and could not be measured with accuracy. The low value found for α is related to the state of the surface, and represents the effective thermal diffusivity of the rough surface and the layer immediately below. This result shows that the PTR method is very sensitive to near-surface thermophysical properties. The value found for S_1 (back 2) is as expected for damaged surfaces; it is also in agreement with the theoretical predictions for bare surfaces (Fig. 4, and Table I). After the mechanical damage on the back surface of the wafer, the recombination lifetime decreased dramatically. This suggests that the carrier recombination lifetime is not only affected by the bulk lifetime, but also by the recombination on the front surface of the sample exposed to the laser beam. This result is consistent with the very shallow optical absorption depth, $\beta^{-1} = 10^{-4}$ cm at 514 nm.[26] Under front-surface detection, the very-near-surface photoinjected carrier lifetime may be affected by the electronic state of the surface itself. The effective lifetime, τ_{eff}, is known to be given by[27]

$$\frac{1}{\tau_{eff}} = \frac{1}{\tau_b} + \frac{1}{\tau_s} \qquad [8]$$

where τ_b is the bulk lifetime, and τ_s represents the surface lifetime. It is possible that the PTR-measured lifetime under 514 nm laser irradiation is more closely related to τ_s, rather than to τ_b. Measurements at longer wavelengths and greater optical absorption depths are likely to be more representative of bulk lifetime, as shown in our earlier work.[28]

Therefore, according to the results from the high-resistivity sample (wafer no. 30), Fig. 8 and Table III, the state of the back surface plays an important role in determining the recombination carrier lifetime.[22] Under high surface passivation, it is possible to obtain the bulk lifetime from our measurements. Daio *et al.*[27] measured the effective bulk and surface lifetimes in CZ n-Si samples using the photoconductance decay (PCD) method before and after thermal oxidation as a function of temperature (20 to 250°C). These authors found the effective lifetime for the bare samples to be about 40 μs and 1000 μs before and after the thermal process, respectively. According to Eq. 8 the effective lifetime in bare samples is mainly attributed to the surface lifetime, since $1/\tau_b << 1/\tau_{eff}$, thus $\tau_{eff} \sim \tau_s$. The theoretical best fit to the amplitude and phase data obtained from the back surface (after scratching) in Fig. 8 is not satisfactory for frequencies above 1 kHz. The reason is probably the highly inhomogeneous nature of the damage inflicted on the site, which cannot

Table III. Thermal and electronic transport parameters for long lifetime p-Si (sample no. 30), determined by 3D PTR model and the multiparameter best fit; intact sample (front 1, back 1); and scratched back surface (front 2, back 2).

	Amplitude (mV)	α (cm^2/s)	τ (μs)	D_n (cm^2/s)	S_1 (cm/s)	S_2 (cm/s)	C_p (a.u)	C_t (a.u)
Front 1	56.652	0.96	950	3.2	90	—	4.5×10^{-20}	3.1
Back 1	66.505	0.96	950	3.2	110	—	4.5×10^{-20}	3.0
Front 2	37.388	0.96	80	3.2	90	—	0.15×10^{-20}	2.0
Back 2	12.776	0.12	12	3.2	3×10^6	—	3.0×10^{-23}	1×10^{-4}

Downloaded 21 Jul 2008 to 128.100.49.17. Redistribution subject to ECS license or copyright; see http://www.ecsdl.org/terms_use.jsp

S0013-4651(99)05-082-X CCC: $7.00 © The Electrochemical Society, Inc.

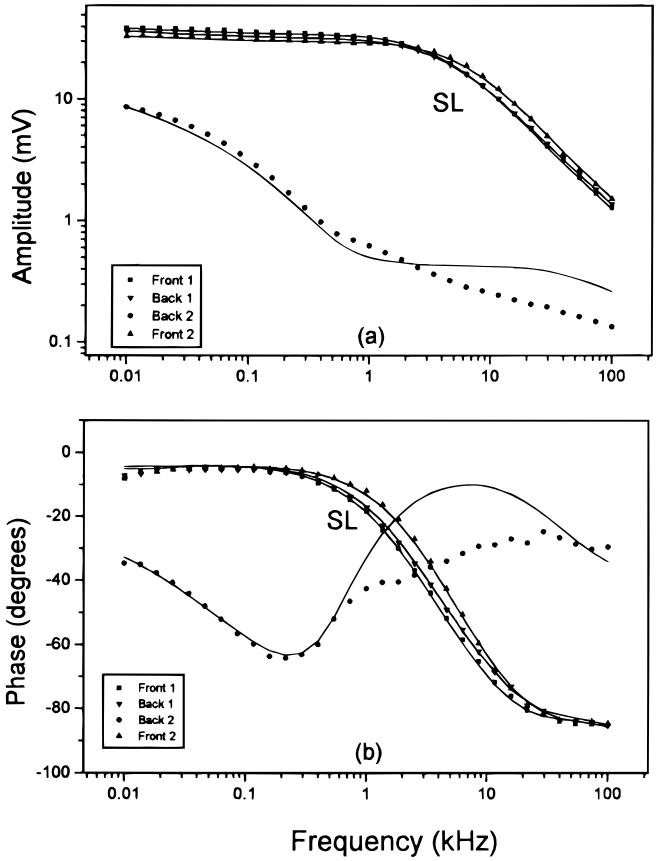

Figure 9. PTR signal amplitude (a) and phase for a Si sample with short-lifetime wafer no. 6, before (front 1 and back 1) and after (front 2 and back 2) damage, respectively.

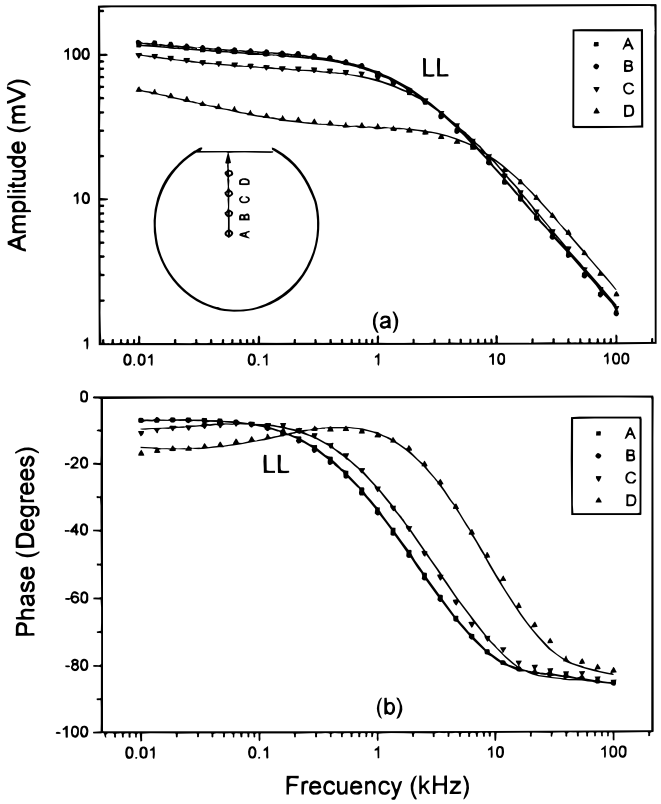

Figure 10. PTR signal amplitude (a) and phase (b) for four positions along the radial directions in Si sample with long-lifetime wafer no. 30. The inset in Fig. 10a shows each radial coordinate location.

be fitted with an axially homogeneous theory. Our earlier inhomogeneous plasma-wave theoretical approach to this problem may be appropriate in this case.[29]

A low resistivity p-Si (sample no. 6) was also subjected to a similar scratching damage. The experimental PTR signal amplitude and phase are shown in Fig. 9. The solid squares and inverted triangles represent the experimental values before scratching; the solid lines represent the best-fitted curves to the experimental data. The parameters found for this wafer when probed from the front and back surface are shown in Table IV. The observed trends in these results are similar to those obtained from the high-resistivity, long-lifetime wafer. After the mechanical damage, a strong change was found in the effective recombination lifetime (20 times smaller that the original lifetime). The effective thermal diffusivity also shows a dramatic change due to the change in the state of the surface. These results are consistent with the generation of mechanical surface and near-surface defects at the damage sites, which act as both thermal interfaces/boundaries impeding heat flow, as well as electronic recombination centers trapping free photoinjected carriers. The disagreement between experimental data and theoretical fits at the high frequency regarding the damaged site is consistent with a high degree of depth inhomogeneity of the damage profile.

Radial scans.—Four positions along the radial direction were measured perpendicular to the flat for the high- (sample no. 30) and low-resistivity (sample no. 5) p-Si wafers: at the center point (A); at 1.8 cm (B); at 3.6 cm (C); and at 5.4 cm from center (D); see inset in Fig. 10a. In Fig. 10 the solid symbols represent the experimental values while the solid lines represent the best-fitted theoretical curve for each radial position. A summary of the thermal and electronic parameters determined by this procedure for each point on the high resistivity wafer (no. 30) is given in Table V. These results indicate that there is a direct relation between PTR signal amplitudes and lifetime values as expected from the simulations of Fig.1. When the PTR signal increases, so does the lifetime. A plot of this relationship is shown in Fig. 11. This essentially linear relationship can be used as a rapid wafer inspection method, or for the nondestructive evaluation of industrial silicon wafers through scanning lifetime imaging. Based on this linear relationship, Fig. 12 shows amplitude and phase PTR images of the high-resistivity Si wafer (no. 30) probed from the front (intact) surface and scanned over the coordinates of the back-surface region with the mechanical damage. The frequency chosen was 5 kHz, corresponding to an optimal phase resolution of the de-

Table IV. Thermal and electronic transport parameters for short lifetime p-Si (sample no. 6), determined by 3D PTR model and the multiparameter best fit; intact sample (front 1, back 1); and scratched back surface (front 2, back 2).

	Amplitude (mV)	α (cm^2/s)	τ (μs)	D_n (cm^2/s)	S_1 (cm/s)	S_2 (cm/s)	C_p (a.u)	C_t (a.u)
Front 1	38.729	0.78	200	8.3	115	—	1.9×10^{-21}	0.14
Back 1	36.590	0.78	200	8.3	210	—	2.1×10^{-21}	0.14
Front 2	33.010	0.78	87	8.3	110	—	1.8×10^{-21}	1.10
Back 2	8.636	0.15	4	—	7×10^5	—	1.0×10^{-21}	3×10^{-4}

Downloaded 21 Jul 2008 to 128.100.49.17. Redistribution subject to ECS license or copyright; see http://www.ecsdl.org/terms_use.jsp

S0013-4651(99)05-082-X CCC: $7.00 © The Electrochemical Society, Inc.

Table V. Thermal and electronic transport parameters for high-resistivity p-Si (sample no. 30), determined by the 3D PTR model and the best-fit multiparameter procedure.

	Amplitude (mV)	α (cm^2/s)	τ (μs)	D_n (cm^2/s)	S_1 (cm/s)	S_2 (cm/s)	C_p (a.u)	C_t (a.u)
A	116.81	0.96	1400	3.1	185	—	7.3×10^{-21}	0.40
B	120.92	0.96	1555	3.1	170	—	7.3×10^{-21}	0.40
C	99.601	0.80	605	4.9	170	—	1.1×10^{-20}	1.10
D	56.967	0.75	50	8.2	330	—	8.0×10^{-22}	2.0

fect as indicated in the frequency scans of Fig. 8. It is seen that the position of the underlying damage is well resolved in both images, with the phase image showing the expected higher sensitivity in terms of a greater extent of the damage region compared to the amplitude image. Based on the linear relationship of Fig. 11, we are justified in suggesting that the change in carrier lifetime is the major contrast mechanism in Fig. 12, which can thus be calibrated and labeled as a free-carrier recombination lifetime image. It is interesting to note the long-range effects of the back-surface mechanical damage throughout the bulk, reaching the front surface of the wafer where devices are fabricated, as captured by the PTR depth-profiling phase image.

Returning to the radial scans, the lifetime and thermal diffusivity values at, or close to, the center (A, B) are larger than those (C, D) closer to the edge of these Si wafers (high resistivity, Table V). The opposite trend is observed for the front surface recombination velocity. This may be related directly to the crystal growth process along the radial position of the large size industrial Si wafers. Therefore, PTR diagnostics proves to be a suitable tool for investigating variations in the manufacturing quality of Si wafers and its impact on the electronic and thermophysical properties of the surface. Both properties are central to controlling the electronic and thermal behavior of devices to be fabricated on the wafer. Similarly, a radial scan was performed on the low-resistivity wafer (no. 6). The PTR signal amplitude and phase are shown in Fig. 13. A summary of the different parameters determined by the multiparameter fitting procedure is given in Table VI. The measured values of these parameters at radial locations (A-D), and the proximity of the frequency curves in Fig. 13, indicate that this wafer is more homogeneous than the high-resistivity wafer of Table V. However, inspection of C_p and C_t values reveals that this sample has an overall smaller plasma component than the high resistivity wafer, with the exception of the center point. As a general rule it was found that the lifetime values associated with low-resistivity wafers in our extended study of 40 wafers were substantially shorter that those of the higher resistivity wafers. It was also found that, in general, there is an inverse correlation between lifetime and surface recombination velocity, with low-resistivity wafers exhibiting higher front surface recombination velocities than their high-resistivity counterparts.

Points C and D of the high-resistivity wafer exhibited positive PTR signal transients (+6%) while the low-resistivity wafer exhibited negative transients at some locations (−4.46%). An interesting phenomenon about this sample was that not all probed positions on the surface exhibited a transient. Positive transient phenomena have been previously observed with industrial Si wafers. They have been associated with laser annealing of low activation energy surface defects, and the concomitant improvement in surface recombination velocity.[14] Negative transients are currently under investigation and the results will be reported in a future publication.

Conclusions

A reliable multiparameter fit computational procedure has been developed to measure primary transport properties of Si wafers from frequency-domain PTR signals. The question of the uniqueness of the fit and of the effects of each electronic transport parameter on the PTR frequency curves was addressed in detail. Experimental data were generated from high- and low-resistivity 6 in. Si wafers, and multiparameter fits were carried out to test the fitting procedure. As a result, up to seven different transport parameters can be measured: five of these are intrinsic parameters and are related to the electron-

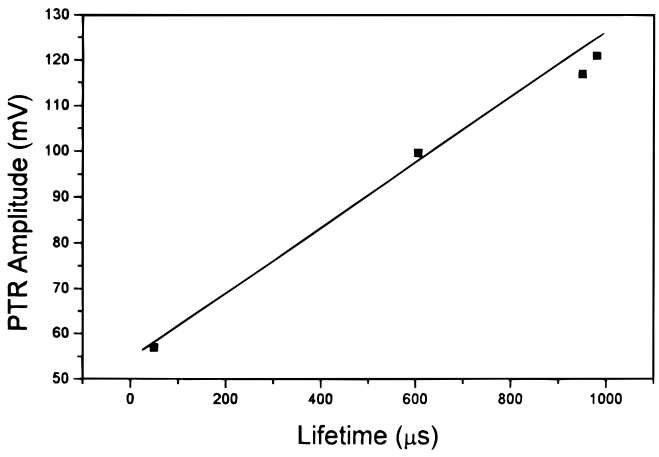

Figure 11. Linear relation between lifetime measurements and PTR signal amplitude for the high-resistivity p-Si wafer no. 30, evaluated at four different positions along the radial direction.

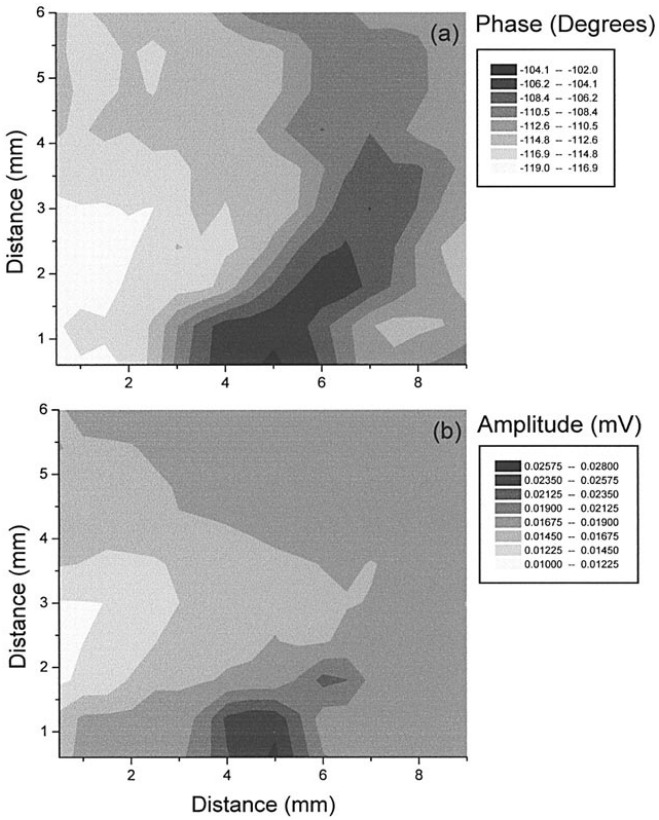

Figure 12. Amplitude (a) and phase (b) PTR images of the long-lifetime Si wafer no. 30, probed from the front (intact) surface and scanned over the coordinates of the back surface mechanical defect site.

Downloaded 21 Jul 2008 to 128.100.49.17. Redistribution subject to ECS license or copyright; see http://www.ecsdl.org/terms_use.jsp

S0013-4651(99)05-082-X CCC: $7.00 © The Electrochemical Society, Inc.

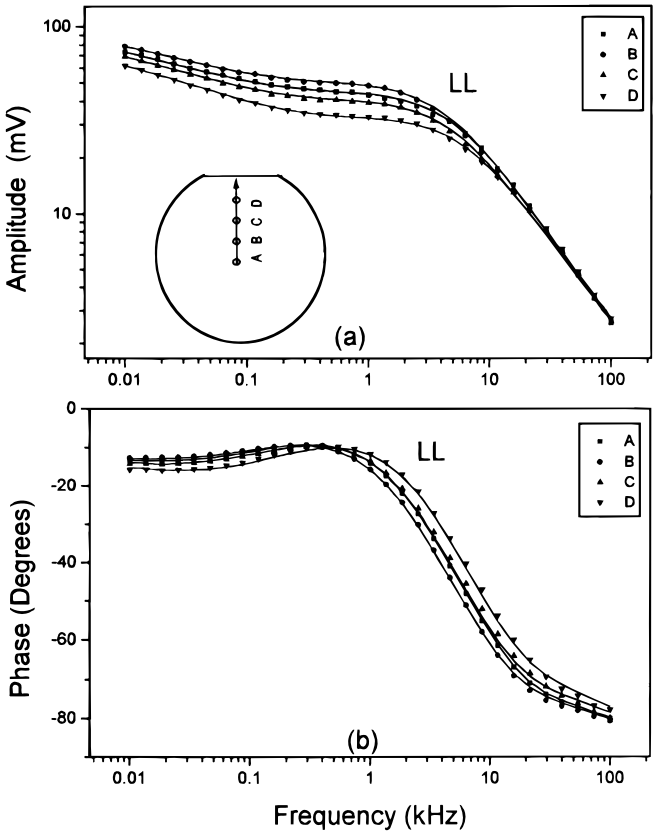

Figure 13. PTR signal amplitude (a) and phase (b) for four positions along the radial directions in a Si sample (wafer no. 6) with short lifetime.

ic and thermal transport properties of laser photoinjected carriers in semiconductors. The other two, C_t and C_p, are extrinsic (empirical) parameters. For this particular set of samples, however, the low back surface recombination velocity could not be determined, since the values obtained from the fitting procedure were below the PTR sensitivity values.

The major conclusions of PTR signal simulations and multiparameter fits to the Si wafers used in this work (and many others from the same batch) clearly show that there is a strong correlation between nominal resistivity, front-surface recombination velocity, and recombination lifetime: higher resistivity wafers are likely to have lower surface recombination velocity and longer lifetimes. Overall, over the entire set of 40 wafers tested in the course of this investigation, the PTR lifetime was found to be a more consistent and sensitive measure of the electronic quality of the wafers than the surface recombination velocity and the other fitted parameters. This is expected, since the former is a measure of subsurface quality due to rapid carrier diffusion before recombination, whereas the latter is strongly affected by surface processing and handling conditions. Nevertheless, evidence of the PTR lifetime dependence on the state of the wafer surface has also been observed with deliberately damaged samples. Therefore, PTR lifetimes measured under 514 nm laser irradiation are likely, to be near-surface recombination values of the effective lifetime, Eq. 8. Longer wavelengths will be needed to probe the true bulk lifetime. The monotonic relationship of the PTR amplitude to the recombination lifetime, which was predicted earlier[3] and emerged from our data, Fig. 11 and 12, offers a potentially valuable tool for remote, noncontact, nondestructive, and rapid surface lifetime mapping of process wafers. The lattice thermal contribution was found to have some influence at low frequencies < 1000 Hz. The carrier plasma contribution, however, dominates the signal throughout the high modulation frequency for both high- and low-resistivity wafers.

Acknowledgments

The continuing support of this project by Materials and Manufacturing Ontario (MMO), a Province of Ontario Center of Excellence, is gratefully acknowledged. One of the authors (M.E.R.) wishes to acknowledge Centro de Investigación en Ciencia Aplicada y Tecnologia Avanzada (México) and COLCIENCIAS (Colombia) for their partial support.

The University of Toronto assisted in meeting the publication costs of this article.

Appendix

The Hankel integral required in Eq. 1-6 is an improper integral, *i.e.*, its upper limit is infinite. It is assumed that the integral exists and approaches a finite value as the upper limit of integration approaches infinity. This assumption is based on the physical quantity represented by the integrand. Equation 1 was calculated using the improper integral routine, *qromo*[30] with *midpnt* taken from *Numerical Recipes in C*.[30] The routine solves for smooth integrals with an upper limit to infinity using Romberg integration in a semi-open interval. In calculating improper integrals the convergence criterion has to be carefully met. A convenient convergence approach for this integral is to replace the infinite upper limit with a finite value b and to evaluate the integral with increasing values of b until any further increase in b results in a negligible change in the integral. The downfall of this approach is that the value b is chosen according to the integrand behavior, which in turn depends on the input parameters. If the integrand is not tested for convergence each time an input parameter is changed, an error can occur. To avoid this rigorous procedure the additional routine *midinf*,[30] which maps an infinite range of integration to a finite one using the identity

$$\int_a^b f(x)dx = \int_{1/b}^{1/a} \frac{1}{t^2} f\left(\frac{1}{t}\right)dt \qquad \text{[A-1]}$$

is used. As a result, the Hankel integral is separated into two integrals

$$\int_0^\infty f(x)dx = \int_0^b f(x)dx + \int_{1/1\times10^{30}}^{1/b} \frac{1}{t^2} f\left(\frac{1}{t}\right)dt \qquad \text{[A-2]}$$

where the first integral is calculated using the *midpnt* routine from 0 to b and the second integral is calculated using the *midinf* routine from b to large number (1×10^{30}). This type of methodology assures that the convergence criterion is reached every time, provided b is large enough so that the integrand begins to approach its asymptotic decrease.

References

1. S. J. Sheard, M. G. Someckh, and T. Hiller, *Mater. Sci. Eng. B*, **5**, 101 (1990).
2. M. Hiller, M. G. Somekh, S. J. Sheard, and D. R. Newcombe, *Mater. Sci. Eng. B*, **5**, 107 (1990).
3. A. Mandelis, *Solid State Electron.*, **42**, 1 (1998).
4. A. Salnick, A. Mandelis, H. Ruda, and C. Jean, *J. Appl. Phys.*, **82**, 1853 (1997).
5. A. Salnick, A. Mandelis, and C. Jean, *Appl. Phys. Lett.*, **611**, 17 (1996).
6. T. Ikari, A. Salnick, and A. Mandelis, *J. Appl. Phys.*, **85**, 7392 (1999).

Table VI. Thermal and electronic transport parameters for low-resistivity p-Si (sample no. 6), determined by the 3D PTR model and the best-fit multiparameter procedure.

	Amplitude (mV)	α (cm^2/s)	τ (μs)	D_n (cm^2/s)	S_1 (cm/s)	S_2 (cm/s)	C_p (a.u)	C_t (a.u)
A	73.201	0.75	95	5.50	480	—	8.0×10^{-21}	0.840
B	78.663	0.78	120	5.50	450	—	1.05×10^{-22}	0.834
C	68.997	0.75	95	5.20	540	—	7.0×10^{-22}	0.834
D	61.918	0.75	60	5.30	630	—	9.7×10^{-22}	2.60

Downloaded 21 Jul 2008 to 128.100.49.17. Redistribution subject to ECS license or copyright; see http://www.ecsdl.org/terms_use.jsp

S0013-4651(99)05-082-X CCC: $7.00 © The Electrochemical Society, Inc.

7. W. Shockley and W. T. Read, *Phys. Rev.*, **87**, 835 (1952).
8. W. M. Bullis and H. R. Huff, *J. Electrochem. Soc.*, **143**, 1399 (1996).
9. P. Spirito and A. Sanseverino, *Solid-State Electron*, **37**, 1429 (1994).
10. S. Daliento, A. Sanseverino, P. Spirito, P. M. Sarro, and L. Zeni, *IEEE Electron Device Lett.*, **EDL-17**, 148 (1996).
11. K. D. Cummings, S. J. Pearton, and G. P. Vella-Coleiro, *J. Appl. Phys.*, **60**, 1676 (1986).
12. G. Zoth and W. Bergholz, *J. Appl. Phys.*, **67**, 6764 (1990).
13. S. Sheard and M. Somekh, in *Non-Destructive Evaluation*, A. Mandelis, Editor, Chap. 5, Prentice-Hall, Englewood Cliffs, NJ (1994).
14. M. E. Rodriguez, J. A. Garcia, A. Mandelis, Y. Riopel, and C. Jean, *Appl. Phys Lett.*, **74**, 2429 (1999).
15. A. Pinto Neto, H. Vargas, N. F. Leite, and L. C. M. Miranda, *Phys. Rev. B.*, **41**, 9971 (1990).
16. A. Salnick, A. Mandelis, F. Funak, and C. Jean, *Appl. Phys. Lett.*, **71**, 1531 (1997).
17. T. Yoshida and Y. Kitagawara, in *High Purity Silicon V*, C. L. Claeys, P. Rai-Choudhury, P. Stallhofer, and J. E. Maurits, Editors, PV 96-13, p. 455, The Electrochemical Society Proceedings Series, Pennington, NJ (1996).
18. A. Cuevas, P. A. Basore, G. Giroult-Matlakowki, and C. Dubois, *J. Appl. Phys.*, **80**, 3370 (1996).
19. E. Yablonovich, D. L. Allada, C. C. Chang, T. Gmitter, and T. B. Bright, *Phys. Rev. Lett.*, **57**, 249 (1986).
20. E. Yablonovitch, R. M. Swanson, W. D. Eades, and B. R. Weinberg, *Appl. Phys. Lett.*, **48**, 245 (1986).
21. A. Coreira, D. Ballutaud, and A. Boutri-Forveille, *Appl. Phys. Lett.*, **66**, 2394 (1995).
22. A. W. Stephens and M. A Green, *J. Appl. Phys.*, **8**0, 3897 (1996).
23. D. A. Ramappa and W. B. Henley, *Appl. Phys. Lett.*, **72**, 2298 (1998).
24. J. Lagowski, P. Edelman, M. Dexter, and W. B. Henley, *Semicond. Sci. Technol.*, **7A**, 185 (1992).
25. J. Lagowski, V. Faifer, and P. Edelman, in *High Purity Silicon IV*, C. L. Claeys, P. Rai-Choudhury, P. Stallhafer, and J. E. Maurits, Editors, PV 96-13, The Electrochemical Society Proceedings Series, Pennington, NJ (1996).
26. A. Dargys and J. Kundrotas, *Handbook on Physical Properties of Ge, Si, GaAs and InP*, p. 811, Science and Encyclopedia Publ., Vilnius, Lithuania (1994).
27. H. Daio, A. Buczkowski, and F. Shimura, *J. Electrochem. Soc.*, **141**, 1590 (1994).
28. A. Mandelis, R. Bleiss, and F. Shimura, *J. Appl. Phys.*, **74**, 3431 (1991).
29. A. Salnick and A. Mandelis, *J. Appl. Phys.*, **80**, 5278 (1996).
30. W. H. Press, S. A. Teukolsky, W. T. Vetterling, and B. P. Flannery, *Numerical Recipes in C*, 2nd ed., Cambridge University Press, Cambridge (1992).

Downloaded 21 Jul 2008 to 128.100.49.17. Redistribution subject to ECS license or copyright; see http://www.ecsdl.org/terms_use.jsp